

HYBRID METHOD OF HIGHER-ORDER MOM AND NYSTRÖM DISCRETIZATION PO FOR 3D PEC PROBLEMS

B. Lai, N. Wang, H.-B. Yuan, and C.-H. Liang

National Key Laboratory of Science and Technology
on Antennas and Microwaves
Xidian University, Xi'an, China

Abstract—This paper presents an efficient and accurate hybrid approach of method of moments (MoM) and physical optics (PO) for radiation problems such as antennas mounted on a large platform. The new method employs higher-order hierarchical Legendre basis functions in the MoM region and higher-order Nyström scheme in the PO region. The two regions are both discretized with large domains. The unknowns can be much less than those in the small-domain MoM-PO solutions, which will lead to a great reduction in computation complexity. Furthermore, with the Nyström scheme in the PO region, the higher-order accuracy is maintained, and the calculation of the impedances can be more efficient than that in the existing higher-order MoM-PO procedure. Numerical results show the validity of the proposed method.

1. INTRODUCTION

The method of moments (MoM) [1] has been widely used to solve electromagnetic scattering and radiation problems. However, the computational complexity and memory storage of the conventional MoM which leads to a dense system of linear equations are both $O(N^2)$, where N is the number of unknowns. Therefore, the traditional MoM is limited to electrically small problems. To efficiently analyze the large problems in terms of wavelength, hybridization of the MoM with asymptotic techniques [2], such as physical optics (PO) or ray-based geometrical theory of diffraction (GTD) method, has been proposed in the past years. The asymptotic techniques used in large smooth

part of the structure can greatly reduce the computation and storage complexity. Meanwhile, the MoM used in the other parts can keep the accuracy. Accordingly, the hybrid methods have been applied to a wide class of large-scale practical electromagnetic problems.

The current-based technique MoM-PO is an approximation of the hybrid electric field integral equation (EFIE)-magnetic field integral equation (MFIE) formulation. It was firstly applied to 3D structures in [3]. Then, similar MoM-PO approaches can be seen in [4]. The further improvements were presented in [5–7]. These methods all used lower-order current approximation [13], in which the model is discretized with small elements. The average size of the elements is limited to $\lambda/10$, where λ is the wavelength. This will result in a large number of unknowns and then the great requirements of the computation and storage resources. More recently, the higher-order basis functions [9–11] are introduced to the MoM to greatly reduce the number of unknowns, and they are also applied to fast algorithms [12, 13]. The higher-order MoM-PO methods were proposed in [14, 15], in which the number of unknowns has been dramatically reduced by employing the higher-order basis functions which are defined on the relatively large elements. In [15], hierarchical polynomial basis functions based Galerkin technique was used in MoM region, and the modified Chebyshev polynomial basis functions based point-matching technique was used in PO region. However, the computation costs can still be large since each impedance matrix element is obtained by a parametric coordinate based numerical integral. In [16], the MoM-PO procedure is accelerated by the PC cluster. In [17] and [18], the Non-Uniform Rational B-Spline technique (NURBs) technique is introduced to improve the geometry modeling in PO region. In [19, 20], the NURBs technique is also introduced to MoM. The MoM-PO method are also employed to analyze the antenna-radome structure efficiently [21].

The Nyström method is a point-based discretization scheme with approximating the conventional integral through a certain quadrature rule. By employing the locally corrected scheme, the locally corrected Nyström (LCN) method has been used for integral equation methods [22–25]. This scheme can be derived from higher-order MoM solution where both the basis and the testing functions are expanded as a set of smooth functions. Therefore, it can provide the same accuracy as the higher-order basis functions based Galerkin scheme.

This paper presents an efficient higher-order MoM-PO technique to analyze the 3D PEC problems. The higher-order hierarchical Legendre basis functions based Galerkin technique is employed in the MoM region. The Nyström scheme is firstly employed in the PO region.

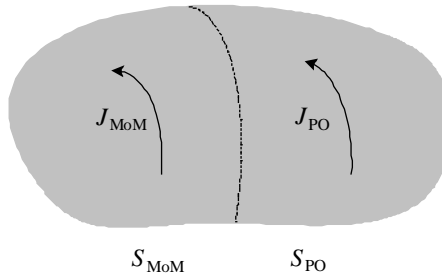


Figure 1. Perfectly conductor decomposed into regions S_{MoM} and S_{PO} .

Like the existing higher-order hybrid methods, the entire model is discretized with electrically large generalized curvilinear quadrilaterals, and the high-order accuracy is kept. However, the new method is more convenient in implementation. Firstly, the PO-PO matrix can be made into an identity matrix more easily. Then, the interactions between the MoM and the PO regions can be calculated more efficiently. Therefore, the computation costs are much less than that in the existing Higher-order MoM-PO scheme.

2. HYBRID MOM-PO PROCEDURE

Consider the problem of radiation and scattering from an arbitrary 3D PEC structure. Using the Schelkunoff's equivalent principle, the conductor can be replaced by the equivalent currents which radiate in the free space. To apply the MoM-PO scheme, we decompose the problem into two regions shown in Fig. 1: The MoM region S_{MoM} , including antennas and near regions, geometrical discontinuities, electrically small structures, etc., and the PO region S_{PO} , including the remaining surfaces.

Applying the boundary conditions to the tangential components of the electric and magnetic fields, we can get a pair of coupled integral equations ([4] and [15])

$$\mathbf{n} \times [\mathbf{E}(\mathbf{J}_{\text{MoM}}) + \mathbf{E}(\mathbf{J}_{\text{PO}}) + \mathbf{E}^i] = 0 \quad (1)$$

in the MoM region, and

$$\mathbf{J}_{\text{MoM}} + \mathbf{J}_{\text{PO}} = 2\mathbf{n} \times [\mathbf{H}(\mathbf{J}_{\text{MoM}}) + \mathbf{H}(\mathbf{J}_{\text{PO}}) + \mathbf{H}^i] \quad (2)$$

in the PO region, where \mathbf{n} is the unit normal vector on the surfaces, \mathbf{E}^i and \mathbf{H}^i represent the incident fields. \mathbf{J}_{MoM} on the left side of (2) only exist in the domain where the MoM region and the PO region overlap.

$\mathbf{E}(\mathbf{J})$ and $\mathbf{H}(\mathbf{J})$ are the scattering fields due to the current \mathbf{J} and are expressed as

$$\mathbf{E}(\mathbf{J}) = -j\omega\mu \int_S \mathbf{J}Gds - \frac{j}{\omega\epsilon} \nabla \int_S \nabla G \cdot \mathbf{J}ds \quad (3)$$

and

$$\mathbf{H}(\mathbf{J}) = \nabla \times \int_S \mathbf{J}Gds \quad (4)$$

with $G = \frac{e^{-jkR}}{4\pi R}$ being the Green's function, where R is the distance of the field point from the source point and k is the free-space wavenumber. For the PO application, (2) is approximated as

$$\mathbf{J}_{\text{MoM}} + \mathbf{J}_{\text{PO}} = \begin{cases} 2\mathbf{n} \times [\mathbf{H}(\mathbf{J}_{\text{MoM}}) + \mathbf{H}^i], & \mathbf{r} \in S_{\text{lit}} \\ 0, & \mathbf{r} \in S_{\text{shad}} \end{cases} \quad (5)$$

where S_{lit} (S_{shad}) denote the lit (shadowed) regions as determined by geometrical optics (GO).

Then, by employing the basis and testing functions in both of the two regions, (1) and (6) can be rewritten as matrix equations

$$\begin{bmatrix} Z_{\text{MoM}}^{\text{MoM}} & Z_{\text{PO}}^{\text{MoM}} \\ Z_{\text{MoM}}^{\text{PO}} & Z_{\text{PO}}^{\text{PO}} \end{bmatrix} \cdot \begin{bmatrix} I_{\text{MoM}} \\ I_{\text{PO}} \end{bmatrix} = \begin{bmatrix} V^{\text{MoM}} \\ V^{\text{PO}} \end{bmatrix}. \quad (6)$$

After simple substitutions, the currents in the two regions can be solved separately by

$$\begin{aligned} & \left[Z_{\text{MoM}}^{\text{MoM}} - Z_{\text{PO}}^{\text{MoM}} (P_{\text{PO}}^{\text{PO}})^{-1} Z_{\text{MoM}}^{\text{PO}} \right] I_{\text{MoM}} \\ & = V^{\text{MoM}} - Z_{\text{PO}}^{\text{MoM}} (P_{\text{PO}}^{\text{PO}})^{-1} V^{\text{PO}} \end{aligned} \quad (7)$$

and

$$I_{\text{PO}} = (P_{\text{PO}}^{\text{PO}})^{-1} [V^{\text{PO}} - Z_{\text{MoM}}^{\text{PO}} I_{\text{MoM}}]. \quad (8)$$

In the higher-order MoM-PO procedure here, both S_{MoM} and S_{PO} are discretized with curvilinear cells with local coordinate system (u, v) . Then, the currents on each domain can be expressed as

$$\mathbf{f}_n(\mathbf{r}) = f^u(u, v)\mathbf{a}_u + f^v(u, v)\mathbf{a}_v \quad (9)$$

where the co-variant vectors \mathbf{a}_u and \mathbf{a}_v are expressed as $\mathbf{a}_u = \partial\mathbf{r}/\partial u$ and $\mathbf{a}_v = \partial\mathbf{r}/\partial v$.

The specific representations of the impedance matrix elements are determined by the choices of the basis and the testing functions and will be described in the following sections. Without loss of generality, we only consider the u -direction components of these functions.

3. HIGHER-ORDER BASIS FUNCTIONS IN THE MOM REGION

In the MoM region, currents are expanded as the higher-order hierarchical Legendre basis functions

$$f^u(u, v) = \frac{1}{J(u, v)} \sum_{i=0}^{M^u} \sum_{j=0}^{M^v} I_{ij}^u \tilde{P}_i(u) P_j(v) \tag{10}$$

where $J(u, v) = |\mathbf{a}_u \times \mathbf{a}_v|$ is the surface Jacobian, I_{ij}^u is unknown coefficient, M^u and M^v are expansion orders along parametric directions, $P_j(v)$ are Legendre polynomials, and $\tilde{P}_i(u)$ are the modified Legendre polynomial [10]. We consider the basis functions in the following simplified form:

$$\mathbf{b}_{ij}^u(u, v) = \frac{\Gamma_{ij}(u, v)}{J(u, v)} \mathbf{a}_u \tag{11}$$

where

$$\Gamma_{ij}(u, v) = \tilde{P}_i(u) P_j(v). \tag{12}$$

By employing the Galerkin scheme for (1) and applying the surface divergence theorem, the impedances corresponding to the testing function defined by indices i_m and j_m on the m th quadrilateral and the basis function defined by indices i_n and j_n on the n th quadrilateral are obtained by

$$z_{\text{MoM}}^{\text{MoM}} = -j\omega\mu \int_{s_m} \int_{s_n} \mathbf{t}_{i_m j_m} \cdot \mathbf{b}_{i_n j_n} G ds_m ds_n + \frac{j}{\omega\epsilon} \int_{s_m} \int_{s_n} \nabla \cdot \mathbf{t}_{i_m j_m} \nabla' \cdot \mathbf{b}_{i_n j_n} G ds_m ds_n \tag{13}$$

where $\mathbf{t}_{i_m j_m}$ denotes the testing function. By transforming the physical space coordinates to the local curvilinear coordinates, we can get

$$z_{\text{MoM}}^{\text{MoM}} = -j\omega\mu \int_{u_1^m v_1^m}^{u_2^m v_2^m} \int_{u_1^n v_1^n}^{u_2^n v_2^n} \int_{u_1^m v_1^m}^{u_2^m v_2^m} \int_{u_1^n v_1^n}^{u_2^n v_2^n} (\Gamma_{i_m, j_m} \mathbf{a}_{u_m}) \cdot (\Gamma_{i_n, j_n} \mathbf{a}_{u_n}) \times G du_m dv_m du_n dv_n + \frac{j}{\omega\epsilon} \int_{u_1^m v_1^m}^{u_2^m v_2^m} \int_{u_1^n v_1^n}^{u_2^n v_2^n} \int_{u_1^m v_1^m}^{u_2^m v_2^m} \int_{u_1^n v_1^n}^{u_2^n v_2^n} \frac{\partial \Gamma_{i_m, j_m}}{\partial u_m} \frac{\partial \Gamma_{i_n, j_n}}{\partial u_n} \times G du_m dv_m du_n dv_n \tag{14}$$

where the integration limits in both quadrilaterals are $u_1 = v_1 = -1$ and $u_2 = v_2 = 1$. When $m = n$, the Duffy transform [26] is employed

to deal with the singularities. The excitation elements in the MoM region can be expressed as

$$v^{\text{MoM}} = - \int_{u_{1m}}^{u_{2m}} \int_{v_{1m}}^{v_{2m}} \Gamma_{i_m, j_m} \mathbf{a}_{u_m} \cdot \mathbf{E}^i du_m dv_m. \quad (15)$$

4. NYSTRÖM SCHEME IN THE PO REGION

4.1. The Nyström Scheme

The mechanism of the Nyström method is replacing the numerical integral with a summation through an appropriate quadrature rule. For example, an integral equation with the linear kernel $K(\mathbf{r}, \mathbf{r}')$ is expressed as follows

$$\phi(\mathbf{r}) = \int_{S'} K(\mathbf{r}, \mathbf{r}') f(\mathbf{r}') dS'. \quad (16)$$

By employing the Gauss-Legendre rule of 2D parametric surface, (16) can be rewritten as

$$\phi(\mathbf{r}) = \sum_{i=1}^{P^u} \sum_{j=1}^{P^v} w_{ij} J_{ij} K(\mathbf{r}, \mathbf{r}_{ij}) f(u_i, v_j) \quad (17)$$

where P^u (P^v) are the number of integral points in u (v) direction, w_{ij} is the integral weight and J_{ij} is the surface Jacobian. Sampling $\phi(\mathbf{r})$ at the integral points will lead to a linear system of equations to solve the unknown coefficients at these points.

However, if the kernel is singular when the source and observation points are on the same quadrilateral, we should employ the locally corrected scheme and rewrite (17) as

$$\phi(\mathbf{r}) = \sum_{i=1}^{P^u} \sum_{j=1}^{P^v} \tilde{w}_{ij} f(u_i, v_j) \quad (18)$$

where \tilde{w}_{ij} are the weights of the specialized local quadrature rule for singularity at \mathbf{r} , and can be explained as the effect of $f(u_i, v_j)$ at \mathbf{r} through the kernel $K(\mathbf{r}, \mathbf{r}_{ij})$. By introducing a set of regular functions $F_s(\mathbf{r})$ ($s = 1, P^u P^v$) distributed on the quadrilateral, we can get \tilde{w}_{ij} by solving the linear system of equations composed of

$$\sum_{i=1}^{P^u} \sum_{j=1}^{P^v} \tilde{w}_{ij} F_s(\mathbf{r}_{ij}) = \int_{S'} K(\mathbf{r}, \mathbf{r}') F_s(\mathbf{r}') dS'. \quad (19)$$

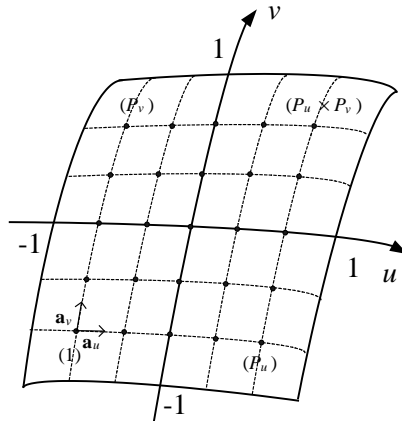


Figure 2. Basis functions distribution on a quadrilateral surface in the PO region.

Thus, the singularities in applying the Nyström scheme have been converted to the singularities of the integrations on the right side of (19). The procedures of dealing these singularities for both the EFIE and the MFIE kernels have been given in [22–24] in detail. Note that the interactions of the points on the two conjoint domains should also be obtained by this locally corrected scheme to maintain the continuity of the currents.

4.2. The Basis and Testing Functions in the PO Region

In the PO region, since there are no singularities in the PO equation, the currents can be simply solved by Nyström scheme with expanding the currents as a set of the Dirac delta functions defined at the integral points as shown in Fig. 2

$$f^u(u, v) = \sum_{i=1}^{P^u} \sum_{j=1}^{P^v} I_{ij}^u w_{ij} J(u_i, v_j) \delta(u - u_i, v - v_j) \quad (20)$$

where I_{ij}^u is unknown coefficient, w_{ij} is the integral weight, $J(u_i, v_j)$ is the surface Jacobian and δ is the Dirac delta function. Similarly, we consider the basis functions in the following simplified form:

$$\mathbf{b}_{ij}^u(u, v) = \mathbf{a}_u w_{ij} J(u_i, v_j) \delta(u - u_i, v - v_j). \quad (21)$$

In dealing with electric field integral equation (EFIE) by the locally corrected procedure mentioned in [22–24], testing functions are as the same as the basis functions. Here in dealing with PO equation,

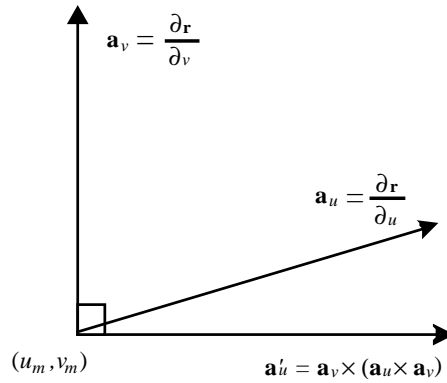


Figure 3. Surface co-variant vectors and the vector of testing function corresponding to the u -direction.

to make $P_{\text{PO}}^{\text{PO}}$ an identity matrix, a proper modification should be made to satisfy

$$P_{\text{PO}}^{\text{PO}} = \frac{1}{2} \int_{S_m} \mathbf{t}_m^{\text{PO}} \cdot \mathbf{b}_n^{\text{PO}} ds_m = \delta_{mn} = \begin{cases} 1, & m = n \\ 0, & m \neq n \end{cases} \quad (22)$$

So we introduce the testing functions as

$$\mathbf{t}_{ij}^u(u, v) = \frac{2\mathbf{a}'_v}{|\mathbf{a}_u \cdot \mathbf{a}'_u|} \frac{\delta(u - u_i, v - v_i)}{w_{ij} J(u_i, v_j)} \quad (23)$$

where

$$\mathbf{a}'_u = \mathbf{a}_v \times (\mathbf{a}_u \times \mathbf{a}_v) \quad (24)$$

as shown in Fig. 3. Evidently, (22) can be simply satisfied.

4.3. The Elements of the MoM-PO Matrix Equation

Using the basis and testing functions described above, we can present the impedance matrix elements of MoM-PO. The projection matrix in the PO region is an identity matrix and expressed as

$$p_{\text{PO}}^{\text{PO}} = \delta(u_{i_m} - u_{i_n}, v_{j_m} - v_{j_n}). \quad (25)$$

The excitation elements in the PO region can be expressed as

$$v^{\text{PO}} = \frac{2\mathbf{a}'_{u_m} \cdot [\mathbf{n} \times \mathbf{H}^i(u_{i_m}, v_{j_m})]}{|\mathbf{a}_{u_m} \cdot \mathbf{a}'_{u_m}| w_{i_m j_m} J(u_{i_m}, v_{j_m})}. \quad (26)$$

From (1) and (3), the elements of $Z_{\text{PO}}^{\text{MoM}}$ are obtained by

$$z_{\text{PO}}^{\text{MoM}} = -j\omega\mu \int_{u_{1m}}^{u_{2m}} \int_{v_{1m}}^{v_{2m}} (\Gamma_{i_m, j_m} \mathbf{a}_{u_m}) \cdot (w_{i_n, j_n} J_{i_n, j_n} \mathbf{a}_{u_n}) \cdot G du_m dv_m - \frac{j}{\omega\epsilon} \int_{u_{1m}}^{u_{2m}} \int_{v_{1m}}^{v_{2m}} (\Gamma_{i_m, j_m} \mathbf{a}_{u_m}) \cdot \nabla(\nabla G \cdot (w_{i_n, j_n} J_{i_n, j_n} \mathbf{a}_{u_n})) du_m dv_m \quad (27)$$

From (4) and (5), the elements of $Z_{\text{PO}}^{\text{MoM}}$ are obtained by

$$z_{\text{MoM}}^{\text{PO}} = \frac{\Gamma_{i_n, j_n}(\mathbf{a}_{u_n} \cdot \mathbf{a}'_{u_m})}{|\mathbf{a}_{u_m} \cdot \mathbf{a}'_{u_m}| w_{i_m, j_m} J(u_{i_m}, v_{j_m}) J(u_{i_n}, v_{j_n})} - \frac{2(\mathbf{a}'_{u_m} \times \mathbf{n})}{|\mathbf{a}_{u_m} \cdot \mathbf{a}'_{u_m}| w_{i_m, j_m} J(u_{i_m}, v_{j_m})} \int_{u_{1n}}^{u_{2n}} \int_{v_{1n}}^{v_{2n}} \nabla G \times (\Gamma_{i_n, j_n} \mathbf{a}_{u_n}) du_n dv_n, \mathbf{r}_n \in S_{\text{lit}} \quad (28)$$

If the MoM and PO regions overlap, the integral kernels of (27) and (28) are singular. In (28), the integrand has a singularity of $O(1/R)$ [24] and can be computed by the Duffy transform. For the integrand in (27), the locally corrected scheme which is a little different from that in [24] should be employed on each overlapped patch. Firstly, we consider (3) and rewrite the kernel as

$$K(\mathbf{r}_m, \mathbf{r}_n) = \mathbf{a}_{u_m} \cdot (-j\omega\mu \bar{\bar{I}} - \frac{j}{\omega\epsilon} \nabla \nabla) G \cdot \mathbf{a}_{u_n}. \quad (29)$$

Then, elements with singularities can be obtained by

$$z_{\text{sig}}(i_m j_m, i_n j_n) = \int_{S_m} \int_{S_n} t_{i_m j_m} K(\mathbf{r}, \mathbf{r}') b_{i_n j_n} ds_m ds_n = \int_{S_m} t_{i_m j_m} K(\mathbf{r}_m, \mathbf{r}_n) w_{i_n j_n} J(\mathbf{r}_n) ds_m = \tilde{w}_{i_n j_n}^{i_m j_m} \quad (30)$$

where $t_{i_m j_m}$ is the higher-order basis function in the MoM region, $b_{i_n j_n}$ is the Dirac delta basis function in the PO region and $J(\mathbf{r})$ is the surface Jacobian at \mathbf{r} . To obtain the specialized quadrature weights $\tilde{w}_{i_n j_n}^{i_m j_m}$, we introduce a set of regular functions $F_{ij}(\mathbf{r})$ defined in the PO region and construct the linear system of equations

$$\sum_{ij} F_{ij}(\mathbf{r}_n) \tilde{w}_{i_n j_n}^{i_m j_m} = \phi_{ij} \quad (31)$$

with the right side part expressed as

$$\begin{aligned}\phi_{ij} &= \sum_{i_n j_n} \int_{S_m} t_{i_m j_m}(\mathbf{r}_m) K(\mathbf{r}_m, \mathbf{r}_n) w_{i_n j_n} J(\mathbf{r}_n) F_{ij}(\mathbf{r}_n) ds_m \\ &= \int_{S_m} \int_{S_n} t_{i_m j_m}(\mathbf{r}_m) K(\mathbf{r}_m, \mathbf{r}_n) F_{ij}(\mathbf{r}_n) ds_m ds_n\end{aligned}\quad (32)$$

By taking $\mathbf{T}_m = t_{i_m j_m}(\mathbf{r}_m) \mathbf{a}_{u_m}$ and $\mathbf{B}_n = F_{ij}(\mathbf{r}_n) \mathbf{a}_{u_n}$, and after simple transformations, we can get

$$\begin{aligned}\phi_{ij} &= -j\omega\mu \int_{S_m} \int_{S_n} \mathbf{T}_m \cdot \mathbf{B}_n G ds_m ds_n \\ &\quad + \frac{j}{\omega\epsilon} \int_{S_m} \int_{S_n} \nabla \cdot \mathbf{T}_m \nabla' \cdot \mathbf{B}_n G ds_m ds_n \\ &\quad + \frac{j}{\omega\epsilon} \int_{L_m} \int_{L_n} (\mathbf{T}_m \cdot \hat{\mathbf{n}}_{l_m}) (\mathbf{B}_n \cdot \hat{\mathbf{n}}_{l_n}) G dl_m dl_n \\ &\quad - \frac{j}{\omega\epsilon} \int_{S_m} \int_{L_n} \nabla \cdot \mathbf{T}_m (\mathbf{B}_n \cdot \hat{\mathbf{n}}_{l_n}) G ds_m dl_n \\ &\quad - \frac{j}{\omega\epsilon} \int_{L_m} \int_{S_n} (\mathbf{T}_m \cdot \hat{\mathbf{n}}_{l_m}) \nabla' \cdot \mathbf{B}_n G dl_m ds_n\end{aligned}\quad (33)$$

where C_m (C_n) are the contour bounding s_m (s_n), and e_m (e_n) are the outward normal to C_m (C_n). Apparently, the integrations are all of $O(1/R)$ singularity and can be efficiently computed by the Duffy transform. Here $F_{ij}(\mathbf{r})$ are chosen the same as the basis functions for the MoM region with only the lower-order basis functions have values on the contour boundary. Note that the line integral didn't exist in (13), that's because each lower-order basis function that spans two domains is taken account as a whole in transforming (3) to (13) and the value of these basis functions on the contour boundary of the entire two domains is zero.

4.4. Advantages of Nyström Discretization in the PO Region

The Nyström scheme can be employed in the PO region to efficiently and accurately calculate the interactions between the currents of the MoM and the PO regions which are the most costly part in the whole procedure. Taking $z_{\text{PO}}^{\text{MoM}}$ as an example, we should consider

the scattered electric field at a point in the MoM region due to the currents in the PO region:

$$\mathbf{E}(\mathbf{r}) = \int_{S'} \bar{\mathbf{G}}(\mathbf{r}, \mathbf{r}') \cdot \mathbf{J}_{\text{PO}}(\mathbf{r}') ds' \quad (34)$$

where $\bar{\mathbf{G}}(\mathbf{r}, \mathbf{r}')$ is the well-known free-space dyadic Green's function, $\mathbf{J}_{\text{PO}}(\mathbf{r}')$ is the current in the PO region, and \mathbf{r} and \mathbf{r}' are the points in the MoM and PO regions, respectively. The computation for filling $Z_{\text{PO}}^{\text{MoM}}$ equals to the summation of computations for (34) at each integral point \mathbf{r} of the testing function in the MoM region.

If polynomial basis functions are employed in the PO region, after introducing the numerical integral, (34) is rewritten as

$$\mathbf{E}(\mathbf{r}) = \sum_n^{N_{\text{PO}}} \sum_i^{N_{\text{F}}} \sum_p^{N_p} w_p J_p \bar{\mathbf{G}}(\mathbf{r}, \mathbf{r}'_p) \cdot \mathbf{f}_i^{\text{PO}}(\mathbf{r}'_p) \quad (35)$$

where \mathbf{r}_p is the p th integral point in the n th PO domain, w_p is the integral weight for parametric surface at \mathbf{r}_p , J_p is the Jacobian of the parametric transformation, and $\mathbf{f}_i^{\text{PO}}(\mathbf{r}'_p)$ is the i th basis function on the n th PO domain.

If the Nyström discretization is employed in the PO region, (34) can be written efficiently as

$$\mathbf{E}(\mathbf{r}) = \sum_n^{N_{\text{PO}}} \sum_p^{N_p} w_p J_p \bar{\mathbf{G}}(\mathbf{r}, \mathbf{r}'_p). \quad (36)$$

Since the basis and testing functions are defined exactly at these integral points, (36) can ensure a great integration accuracy of (34). It has been proved in [24] that the Nyström scheme equals to the higher-order Galerkin scheme in accuracy.

Obviously, under the same accuracy demand of the integral in (34), the computation costs of the new method is N_{F} times less than those for the existing higher-order MoM-PO method where higher-order basis functions are defined in the PO region. When the PO surface is discretized with average one lambda patches, $2 \times 7 \times 7$ Dirac delta functions defined at the integral points are needed at least for Nyström discretization on each patch [24], while $2 \times 5 \times 4$ polynomial basis functions are need at least for higher-order basis functions on each patch [8]. Thus, at this time, the new technique can provide 20 times more computation efficiency. If RWG-like lower-order basis functions are employed, average 300 basis functions should be defined on each one lambda patch. Even only one integral point is used in each triangular patch, the computation costs will be much larger than that

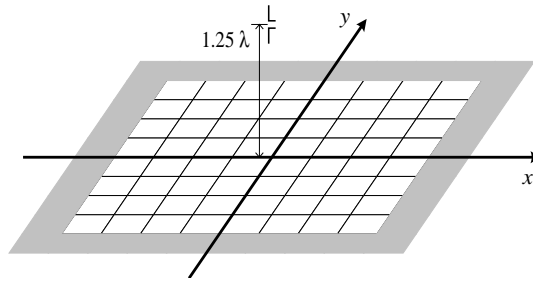


Figure 4. Structure of a dipole near a square plate.

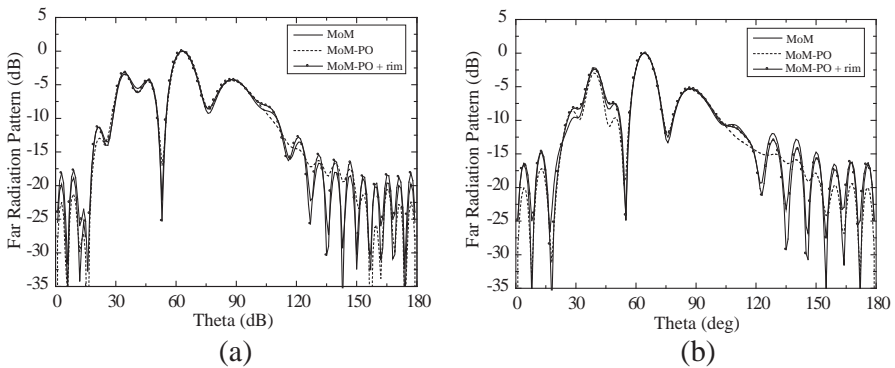


Figure 5. Radiation pattern of the dipole and plate structure in Fig. 4. (a) The plane parallel to a pair of plate edge. (b) The plane containing a plate diagonal.

for Nyström discretization PO method. Although the computation for locally corrected procedure is costly, the overlapped region is small and the whole method is still very efficient.

5. NUMERICAL RESULTS

In this section, three realistic examples are proposed to show the validity of the new method, and all calculations are performed with the double precision arithmetic. The computer used is with Pentium 2.0 GHz CPU and 512 MB ram.

As the first example, we consider a $\lambda/2$ dipole placed on the top of a metallic square plate with 10λ on a side as shown in Fig. 4. The distance from the center of the plate and the antenna is 1.25λ . The wire is with diameter $\lambda/1000$ and is modeled using two segments with second-order current approximation ($M^u = 2$). The plate is discretized with 100 square patches each with λ on a side. The structure is

analyzed using the pure MoM and two hybrid MoM-PO schemes. In the first MoM-PO scheme, the antenna is considered as the MoM region, and the whole plate is considered as the PO region. On each patch, there are 49 discretized points with 7 points in each parametric direction. In the second MoM-PO scheme, we introduce an additional rim of MoM surface elements along the plate edges to improve the accuracy of the hybrid solution. The rim is the shadow region shown in Fig. 5, and a fourth-order current approximation is introduced on it. The normalized radiation patterns in two characteristic planes are calculated with the pure MoM and the two MoM-PO schemes. As shown in Fig. 5, both the two hybrid solutions agree excellent with the MoM solution for angles between 60° and 90° . For other angles, the results obtained by the second hybrid scheme can be better than those by the first one, and the differences between these results and the results obtained by the pure MoM are acceptable. The antenna impedance computed by the first and second MoM-PO are $(78.37, 39.57) \Omega$ and $(78.42, 39.61) \Omega$, respectively, which agree very well with the pure MoM results $(79.05, 40.13) \Omega$.

In the first MoM-PO scheme, the number of unknowns in the MoM region is only 3, and the main computational cost is the filling of the impedance matrices in (8) which costs 3.6 s. With the technique provided in [15], a fourth-order current approximation is introduced in the PO region, the filling time will increase to 28 s. The second MoM-PO scheme requires 1008 MoM unknowns, and the filling time is 713 s. If current approximation in [15] is used, the filling time will increase to be more than one hour. For the second MoM-PO scheme, the memory cost is only 16 MB which is much less than that for the pure MoM procedure. If the plate is considered by pure MoM, 29 800 RWG basis functions are need which will lead to more than 14 GB memory cost. In this paper, the MoM results are obtained by higher-order MoM [10] in which the number of unknowns is 3120 and the memory cost is 156 MB. The matrix filling time is 2471 s which is quite larger than that for MoM-PO procedure.

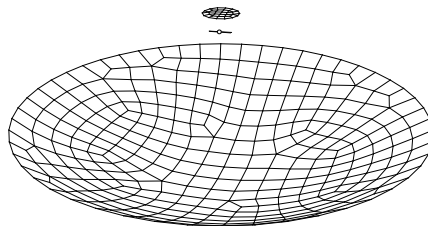


Figure 6. Geometry of a parabolic reflect antennas fed by a dipole backed by a circular dish.

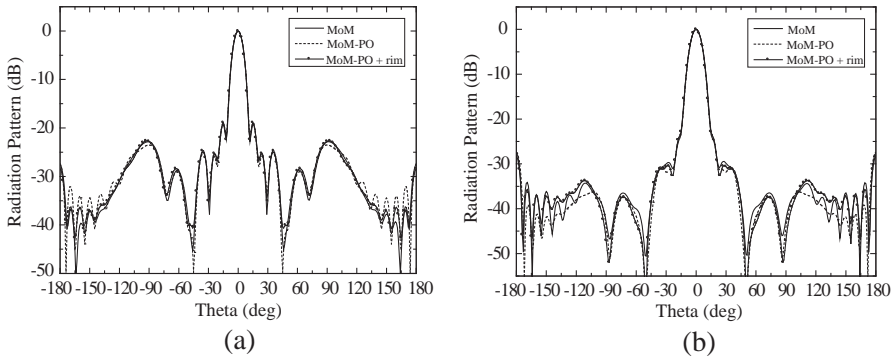


Figure 7. Radiation pattern of the parabolic reflect antennas fed by a dipole backed by a circular dish. (a) *E*-plane. (b) *H*-plane.

The second example deals with a 1.55 GHz parabolic reflector antenna fed by a circular-dish backed dipole [27] as shown in Fig. 6. The reflector is with diameter 1.25 m and focal length 0.419 m, and it is modeled with 304 average side length 0.4λ patches. A 0.2λ dipole is located at the focal point of the reflector. The disk with 5.35 cm radius is 5.74 cm apart at the back of the dipole. The disk and dipole are modeled with 30 average side length 0.02 m flat quadrilaterals. With the MoM-PO procedure, the disk and dipole are considered as the MoM region with the number of unknowns 150, and the reflector is considered as the PO region with 4 discretized points in each parametric direction. As shown in Fig. 7, for angles between -90° and 90° , the results obtained by the hybrid MoM-PO method agree quite well with those obtained by the pure higher-order basis functions based MoM. The filling time of the MoM-PO impedance matrix is 38 s. If a third-order current approximation is used in the PO region [15], the filling time will increase to be 150 s. Fig. 7 also shows the results for a MoM-PO arrangement with a rim in the form of a single layer of MoM patches introduced along the reflector edge. Thus the number of the MoM unknowns is 451, and the filling time is 90 s. By this arrangement, we can get better results for angles larger than 90° . If the polynomial basis functions in [15] are introduced, the filling time will increase to 310 s. The antenna impedances computed by the first and second MoM-PO are $(11.0762, -578.81) \Omega$ and $(11.0893, -579.05) \Omega$, respectively, which agree very well with the pure MoM results $(11.1541, -582.29) \Omega$. In the pure MoM procedure, 2557 higher-order basis functions are employed and the memory cost is 105 MB. However, the memory cost for the MoM-PO procedure is less than 3.3 MB. The matrix filling time for pure MoM is 1392 s which is also quite larger than that for MoM-PO procedure.

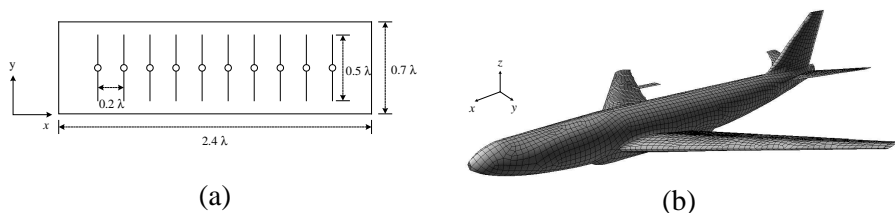


Figure 8. Geometry of (a) the line array and a backed plate and (b) the array mounted on the top of airplane.

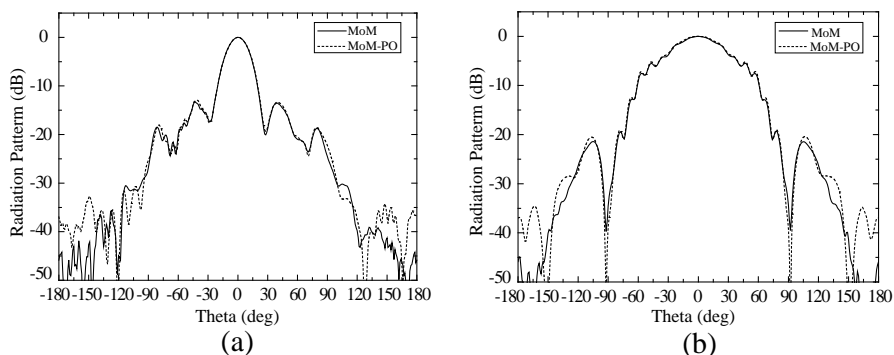


Figure 9. Radiation pattern of a line array mounted on an airplane. (a) *xoz*-plane. (b) *yoz*-plane.

At last, we consider a 1×10 line array working at 150 MHz mounted on the top of an airplane as shown in Fig. 8. The array consists of ten 0.5λ dipoles and is backed with a $0.7\lambda \times 2.4\lambda$ plate. The space distance of two adjacent dipole is 0.2λ . The plate is 0.25λ at the back of array and 1.25λ apart from the airplane. Each dipole is modeled with two segments and the plate is model by 12 plate patches. The plane which is 70.7 meters long and 61.93 meters wide is modeled by 4959 patches with average side length 0.4λ . In the MoM-PO scheme, the array and the plate are considered as the MoM region which leads to 110 unknowns and for each patch of the airplane there are 4 discretized points in each parametric direction. Note that the shadow condition (6) is enforced for each domain in the MoM region. As shown in Fig. 9, the results are compared with those obtained by the higher-order adaptive integral method (AIM) [13]. For angles between -90° and 90° , the two results agree quit well. In the back region, however, the MoM-PO prediction is not accurate enough. This discrepancy is due to the fact that the currents over the shadowed region are week compared to currents in the lit region but contribute significantly to the radiation in the back region of the antenna system. The total computation

time is 510 s with filling time 273 s. The memory cost of MoM-PO procedure is less than 1 MB. Even with higher-order basis, the number of unknowns for pure MoM is still 40011. Although, it can be solved by the AIM, the memory cost is 227 MB and the computation time is nearly 2 hours even with no consideration of the iterative matrix equation solving time.

6. CONCLUSION

In this paper, an efficient higher-order, large domain hybrid MoM-PO procedure has been presented to analyze 3D PEC problems. In the MoM region, higher-order hierarchical Legendre basis functions are introduced to reduce the number of unknowns. In the PO region, a simple Nyström scheme is employed with the currents expanded as a set of Dirac delta functions at the numerical quadrature points. With the new method, the computational costs can be much less than those with the existing higher-order MoM-PO methods.

ACKNOWLEDGMENT

This work was supported in part by the National Science Foundation of China under Grant 60801039 and in part by the Fundamental Research Funds for the Central Universities JY10000902024.

REFERENCES

1. Harrington, R. F., *Field Computation by Moment Methods*, Wiley-IEEE, New York, 1993.
2. Bouche, D. P., F. A. Molinet, and R. Mittra, "Asymptotic and hybrid techniques for electromagnetic scattering," *Proc. IEEE*, Vol. 81, No. 12, 1658–1684, Dec. 1993.
3. Kim, C. S. and Y. Rahmat-Samii, "Low profile antenna study using the physical optics hybrid method (POHM)," *Proc. IEEE Int. Symp. Antennas Propagat. Soc. Meeting*, London, Ont, Canada, Jun. 1991.
4. Hodges, R. E. and Y. Rahmat-Samii, "An iterative current-based hybrid method for complex structures," *IEEE Trans. Antennas Propag.*, Vol. 45, No. 2, 265–276, Feb. 1997.
5. Jakobus, U. and F. M. Landstorfer, "Improved PO-MM hybrid formulation for scattering from three-dimensional perfectly conducting bodies of arbitrary shape," *IEEE Trans. Antennas Propag.*, Vol. 43, No. 2, 162–169, Feb. 1995.

6. Jakobus, U. and F. M. Landstorfer, "Improvement of the PO-MM hybrid method by accounting for effects of perfectly conducting wedges," *IEEE Trans. Antennas Propag.*, Vol. 43, No. 10, 1123–1129, Oct. 1995.
7. Taboada, J. M., F. Obelleio, and J. L. Rodríguez, "Improvement of the hybrid moment method-physical optics method through a novel evaluation of physical optics operator," *Microw. Opt. Technol. Lett.*, Vol. 30, No. 5, 357–363, Sep. 2001.
8. Rao, S. M., D. R. Wilton, and A. W. Glisson, "Electromagnetic scattering by surfaces of arbitrary shape," *IEEE Trans. Antennas Propag.*, Vol. 30, No. 3, 409–418, May 1982.
9. Djordjević, M. and B. M. Notaroš, "Double higher-order method of moments for surface integral equation modeling of metallic and dielectric antennas and structures," *IEEE Trans. Antennas Propag.*, Vol. 52, No. 8, 2118–2129, Aug. 2004.
10. Jørgensen, E., J. L. Volakis, P. Meincke, and O. Breinbjerg, "Higher order hierarchical Legendre basis functions for electromagnetic modeling," *IEEE Trans. Antennas Propag.*, Vol. 52, No. 11, 2985–2995, Nov. 2004.
11. Yuan, H. B., N. Wang, and C. H. Liang, "Fast algorithm to extract the singularity of higher order moment method," *Journal of Electromagnetic Waves and Applications*, Vol. 22, No. 8–9, 1250–1257, 2008.
12. Ding, D.-Z., R.-S. Chen, and Z. Fan, "An efficient sai preconditioning technique for higher order hierarchical mlfmm implementation," *Progress In Electromagnetics Research*, Vol. 88, 255–273, 2008.
13. Lai, B., X. An, H. B. Yuan, N. Wang, and C. H. Liang, "AIM analysis of 3D PEC problems using higher-order hierarchical basis functions," *IEEE Trans. Antennas Propag.*, Vol. 58, No. 4, 1417–1421, Apr. 2010.
14. Jørgensen, E., P. Meincke, and O. Breinbjerg, "A hybrid PO-higher-order hierarchical MoM formulation using curvilinear geometry modeling," *IEEE Antennas and Propagation Soc. Int. Symp. Dig.*, Vol. 4, 98–101, Columbus, OH, Jun. 22–27, 2003.
15. Djordjević, M. and B. M. Notaroš, "Higher-order hybrid method of moments-physical optics modeling technique for radiation and scattering from large perfectly conducting surfaces," *IEEE Trans. Antennas Propag.*, Vol. 53, No. 2, 800–813, Feb. 2005.
16. Zhang, Y., X. W. Zhao, M. Chen, and C. H. Liang, "An efficient MPI virtual topology based parallel, iterative MoM-PO hybrid method on PC cluster," *Journal of Electromagnetic Waves and*

- Applications*, Vol. 20, No. 5, 661–676, 2006.
17. Chen, M., X. W. Zhao, Y. Zhang, and C. H. Liang, “Analysis of antenna around nurbs surface with iterative MoM-PO technique,” *Journal of Electromagnetic Waves and Applications*, Vol. 20, No. 12, 1667–1680, 2006.
 18. Chen, M., Y. Zhang, X. W. Zhao, and C. H. Liang, “Analysis of antenna around NURBS surface with hybrid MoM-PO technique,” *IEEE Trans. Antennas Propag.*, Vol. 55, No. 2, 407–413, Feb. 2007.
 19. Liu, Z.-L. and J. Yang, “Analysis of electromagnetic scattering with higher-order moment method and nurbs model,” *Progress In Electromagnetics Research*, Vol. 96, 83–100, 2009.
 20. Yuan, H. B., N. Wang, and C. H. Liang, “Combining the higher order method of moments with geometric modeling by nurbs surfaces,” *IEEE Trans. Antennas Propag.*, Vol. 57, No. 11, 3558–3563, Nov. 2009.
 21. Hu, B., X.-W. Xu, M. He, and Y. Zheng, “More accurate hybrid po-mom analysis for an electrically large antenna-radome structure,” *Progress In Electromagnetics Research*, Vol. 92, 255–265, 2009.
 22. Canning, L. F., J. J. Ottusch, M. A. Stalzer, J. L. Visher, and S. M. Wandzura, “Numerical solution of the Helmholtz equation in 2D and 3D using a high-order Nyström discretization,” *J. Comput. Phys.*, Vol. 146, No. 2, 627–663, 1998.
 23. Gedney, S. D., “Higher-order method of moments solution of the scattering by three-dimensional PEC bodies using Quadrature based point matching,” *Microw. Opt. Technol. Lett.*, Vol. 29, No. 5, 303–309, Jun. 2001.
 24. Gedney, S. D., “On deriving a locally corrected Nyström scheme from a quadrature sampled moment method,” *IEEE Trans. Antennas Propag.*, Vol. 51, No. 9, 2402–2412, Sep. 2003.
 25. Çalışkan, F. and A. F. Peterson, “The need for mixed-order representations with the locally corrected Nyström method,” *IEEE Antennas and Wireless Propagat. Lett.*, Vol. 2, 72–73, 2003.
 26. Duffy, M. G., “Quadrature over a pyramid or cube of integrands with a singularity at vertex,” *SIAM J. Numer. Anal.*, Vol. 19, No. 6, 1260–1262, Dec. 1982.
 27. Ewe, W. B., L. W. Li, Q. Wu, and M. S. Leong, “Analysis of reflector and horn antennas using adaptive integral method,” *IEICE Trans. Commun.*, Vol. E88-B, No. 6, Jun. 2005.